
Article:
Bryant, MG orcid.org/0000-0003-4442-5169, Buente, D, Oladokun, A et al. (4 more authors) (2017) Surface and subsurface changes as a result of tribocorrosion at the stem-neck interface of bi-modular prosthesis. Biotribology, 10. pp. 1-16. ISSN 2352-5738

https://doi.org/10.1016/j.biotri.2017.02.002

Surface and subsurface changes as a result of tribocorrosion at the stem-neck interface of bi-modular prosthesis

M.G. Bryant, D. Buente, A. Oladokun, M. Ward, G. Huber, M. Morlock, A. Neville

PII: S2352-5738(16)30045-2
DOI: doi:10.1016/j.biotri.2017.02.002
Reference: BIOTRI 42

To appear in: *Biotribology*

Received date: 4 October 2016
Revised date: 6 December 2016
Accepted date: 6 February 2017

Please cite this article as: Bryant, M.G., Buente, D., Oladokun, A., Ward, M., Huber, G., Morlock, M., Neville, A., Surface and subsurface changes as a result of tribocorrosion at the stem-neck interface of bi-modular prosthesis, *Biotribology* (2017), doi:10.1016/j.biotri.2017.02.002

Surface and subsurface changes as a result of tribocorrosion at the stem-neck interface of bi-modular prosthesis.

M. G. Bryant[1], D. Buente[2], A. Oladokun[1], M. Ward[3], G. Huber, M[2]. Morlock[2], A.Neville[1]

1 - Institute of Functional Surfaces (iFS), School of Mechanical Engineering, University of Leeds. UK

2 - Institute of Biomechanics, Hamburg University of Technology. Germany

3 - Institute of Materials Research (IMR), School of Chemical and Process Engineering, University of Leeds. UK

Corresponding Author: M. Bryant (m.g.bryant@leeds.ac.uk)

Institute of Functional Surfaces (iFS), School of Mechanical Engineering, University of Leeds. UK (Permanent Address)

Surface and subsurface changes as a result of tribocorrosion at the stem-neck interface of bi-modular prosthesis.

ABSTRACT

This study presents a detailed multi-scale analysis of the degradation processes occurring on both the CoCrMo and TMZF alloy surfaces at different regions across the taper interface. Co-ordinate measurement machine, scanning electron microscopy, transmission electron microscopy and X-ray Diffraction methods have been utilised to identify the roles of degradation from the mm to nm scale. Dependant on the region of interest, varying topographies and subsurface morphologies were observed across both surfaces. In regions where high pressures are expected, retention of the surface topography was seen on the CoCrMo trunnion. This was complimented by gross shear and plastic deformation of the subsurface material. In regions where maximum penetration was seen, evidence of fretting-corrosion was seen and a loss of the nano-crystalline layer. For the TMZF surface, refinement of the alloy was seen in the top 5 μm, with fatigue cracks within the bulk present. Precipitation and formation of oxide species were observed at depths of 2 μm. The degradation of bi-modular prosthesis is a complex multifactorial process. It is hypothesised that this formation of oxide species at the interface and within the bulk alloy play an important role in the degradation through a combined work-hardening and corrosion process.

1. Introduction

Modular taper interfaces are ubiquitous in modern Total Joint Replacement (TJR). Whilst their initial conception was to enable larger intra-operative range of choice of implants and reduced complexity of the surgical procedure, the introduction of such interfaces has proved problematic since the early 1960's [1]. Although modern TJR is considered a generally successful procedure, wear and corrosion at such interfaces is still one factor that can limit the lifetime of the prosthesis [2-5]. High revision rates owing to Adverse Reaction to Metal Debris (ARMD) and pseudotumour formation have been linked to metal ion release associated with the modular taper interfaces [6,3,5,7].

Bi-modular prostheses have been implicated in higher revision rates owing to metallosis, ARMD and neck fracture [8-10]. Interest into their degradation mechanisms and biomechanics has been renewed due to the public withdrawal and recall of some products [11]. A number of recent publications have detailed the clinical presentation at revision, surface topography and regions in which degradation are commonly found [12-15]. All studies are consistent, reporting that

degradation of the implant is due to wear and corrosion; most present findings from the CoCrMo component in the system.

Buente *et al* [16] recently quantified the material loss from 27 failed Rejuvenate™ prostheses (Figure 1). Material loss of the CoCrMo trunnion was observed. A correlation between total material loss and implantation time was observed with mass loss concentrated on the medial – lateral and anterior – posterior edges and evidence of debris across the surface of the trunnion component (Figure 1). The findings complemented those of Lanting et al [8]. Over the past 20 years extensive research has aimed to elucidate biomechanical, electrochemical, patient and system factors in the ultimate performance of conical modular taper systems [3,17,4,18]. Whilst a lot of work has been conducted in this area a full understanding of the degradation processes occurring within the local regions of the interfaces still does not exist around.

This work presents a detailed evaluation of the surface and subsurface characteristics of a retrieved bi-modular THR, as reported in [16], with the aim of identifying how the combined actions of wear and corrosion affect local surface and subsurface appearance. It also aims to explain why accelerated degradation of the CoCrMo trunnion part is observed when compared to the Ti alloy. Using a variety of different evaluation tools, a detailed view of the degradation processes occurring at modular stem-neck interfaces is assessed across a number of different length scales.

2. Methods

2.1. Implant type

A single bi-modular prosthesis (Rejuvenate™, Stryker, USA), was evaluated in this study. The prosthesis consisted of a dual taper Ti–Mo–Zn-Fe (TMZF™, Stryker, USA) femoral component, and a Co–Cr–Mo (Vitallium™ Stryker, USA) modular femoral neck (Figure 1). Details of implant bearing combination, Goldberg taper score [19] and patient presentation can be found in [16] and can be identified as implant #14. Prior to evaluation surfaces were subjected to sterilisation wash and degreasing with acetone.

2.2. Surface metrology analysis

In order to assess the location and distribution of tribocorrosion degradation occurring on both surfaces at the interface, tactile measurements of both the trunnion and taper portions were obtained using a co-ordinate measurement machine (CMM) and evaluated using methods and algorithms presented in [16]. The contours developed as a result aided the selection of areas in which to focus attention. Areas that presented regions of high, low and no deviation in depth about the reference plane were of interest. In addition localised areas of retained topography in regions of high wear (ie high gradients between degraded and non-degraded) were also of interest.

2.3. X-ray Diffraction Analysis (XRD)

XRD analysis was conducted to in an attempt to identify the crystalline nature of the alloys and to assess if any changes atomic arrangement or increase in residual strain within the microstructure had occurred due to the wear and corrosion processes. These were conducted on both alloys in regions of interest. An approximate volume of 5 mm x 2 mm x 4-6 μm deep (based on instrument used) was evaluated in all cases representing an average of the subsurface in a particular area. 2θ scans between 10° and 60° were carried out using Cu Kα radiation (X'Pert3, PANlytical, Almelo Lelyweg, Netherlands). The scan range selected allows the unambiguous determination of the coexistence of any organic or metallic phases. All scans were taken a minimum of three times. XRD measurements allow the quantification of bulk crystalline state at approximately 2-5 μm depth.

2.4. Electron Microscopy and Chemical Evaluation

Areas of particular interest were subsequently observed under both Scanning and Transmission Electron Microscopes (SEM/TEM) to facilitate image on the mm-μm and nm scale respectively. SEM analysis was conducted using a Carl EVO MA15 and Supra 55 VP FEG-REM (Ziess, Hamburg, Germany). Both microscopes were equipped with Energy Disperse X-ray Spectroscopy (EDS) to facilitate elemental analysis.

To facilitate nano-scale evaluation of the surface and subsurface, a Focused Ion Beam (FIB) preparation method and subsequent TEM and EDX analysis was conducted. This was done according to the method outlined by Bryant *et al* [20]. FIB sections were taken from regions of

interest on both trunnion and taper components with effort made to ensure that the mating surface were analysed from each component. Reference samples were prepared from surfaces of the same implant that had undergone the same manufacturing processes as those in contact at the interface but had not been subjected to the mechanical or crevice corrosion conditions established within the interface (i.e. surface not within the interface). Indexed diffraction patterns with associated miller indices can be found in the supporting materials.

For the CoCrMo trunnion component, all analysis was conducted on an as-received component (i.e. no sectioning required due to its size). To facilitate electron microscopy and FIB preparation methods, the TMZF taper surface was sectioned using two methods. Wire erosion was used where local heating of the local surfaces was not deemed to be an issue (i.e. bulk sectioning and areas of interest of reasonable distance away from cut surface). For surfaces in which local heating was not desirable a MCS 300 Laser-MicroJet Cutter (Synova, Switzerland) was employed to eliminate any thermal damage which may be induced.

3. Results

3.1. CoCrMo Trunnion Analysis

3.1.1. Surface deviations

CMM contour plots are shown in Figure 2 for the CoCrMo trunnion component. Material loss varied as a function of the interface height and angle. High amounts of material loss was observed at the proximal-medial edges of the CoCrMo trunnion. A preserved patch of material was observed, surrounded by regions of high wear. Three areas of interest were highlighted by the CMM analysis and subject to further examination. These are indicated on Figure 2 and described as: 1 – Reference (i.e. unworn material outside the region of contact), 2 – Retained patch (i.e. localised region within the highly worn area where original topography was retained) and 3 – Highly worn (i.e. regions of highest material loss). The taper component was also analysed in the same regions. Details of this particular patient can be found in [16] (Patient 4).

3.1.2. SEM Analysis

Figure 3 demonstrates the surface topographies observed on the CoCrMo trunnion component at revision. A number of different topographies existed due to the different contact conditions established at the interface; a result of the local variations in device geometry, surgical placement and loads established during daily activities. These range from the original machined topography (Figure 3a, Figure 2 region 1), regions that depicted evidence of fretting-corrosion (Figure 3b and c, Figure 2 region 3) and areas that seemingly retained the original machined surfaces whilst surrounded by regions of high wear (Figure 3 d-f, Figure 2, region 2). In regions where surface topography was seemingly retained (Figure 2, region 2), a 'wrinkled' type surface morphology was observed. Localised areas of debris emanating from the TMZF taper component was observed on the patch area (Figure 3e-f, Figure 2 region 2). This was confirmed using EDS analysis as presented in section 3.1.5. In regions in which fretting corrosion was observed, scalloping and directionality of the surface was observed.

3.1.3. XRD Analysis

Figure 4 presents the XRD driffractograms of the CoCrMo trunnion in areas of no measurable wear and those that demonstrated high wear (Figure 2). Due to the geometry and localisation of the medial patch observed in this type of prosthesis XRD plots could not be obtained in these areas. It could be seen that both FCC and HCP phases existed within the alloy: an observation reported extensively within the literature. From the XRD spectra, no significant differences in subsurface crystallinity or excessive amounts of strain within the lattice were observed by shifts in peak position (strain effect) or broadening (changes in crystallite size). This is likely due to the sampled area size, the inability to locally probe regions of high degradation and the possibility of preferred texture/orientation of the crystalline structure.

3.1.4. TEM analysis: Reference Surface

Figure 5 shows bright field images and electron diffraction data for the CoCrMo section prepared from the unworn, undamaged area of the implant (Figure 2, area 1). Figure 5a shows the top 5 μm of the CoCrMo alloy surface. It can be seen that within the top 250 nm of the surface, a nano-crystalline region exists. This is typified by the ringed diffraction pattern inset in Figure 5b.This was

indexed as a Hexagonal Close Packed (HCP) atomic structure and, as detailed in literature; arises from the strain induced transformation (SIT) from the manufacturing processes. Evidence of a Cr and O rich oxide film was also observed at the interface and confirmed with EDX analysis (Figure 5c and 5e, between the red dashed lines). Towards the subsurface, a regular cellular structure was observed (Figure 5d). Electron diffraction indicated that the atomic packing was Face Centred Cubic (FCC). Evidence of shear banding (localised areas of shear strain) and the formation of ε-martensite was observed (Figure 5a and d). This is further supported by the angular streaking of the electron diffraction image; characteristic of lattices containing high strain.

3.1.5. TEM analysis: Retained Patch

Figure 6 shows bright-field TEM and electron diffraction analysis of subsections prepared from the patch area of the CoCrMo trunnion component (ie Region 2, Figure 2). It must be noted that this is the area in which surface topography was seemingly retained whilst surrounded by regions of high material loss. Within this region it is hypothesized that a tribological regime with sufficiently high contact pressure and low displacement is established so a stick or partial slip fretting regime exists resulting in a retention of an unworn area and worn gradient across the surface similar to that described by [21]. Figure 6a shows refinement of the microstructure within the top 300 nm, formation of ε-martensite, stacking faults and the presence of twinning when compared to the reference subsection (Figure 5a). Deformation of grains and evidence of directionality was observed within the top micron of the surface (Figure 6b). Bulk single crystals being sheared to form a nano-crystalline layer was observed in the absence of any visible ε-martensite. This correlated with the direction of joint loading.

Electron diffraction analysis was taken in three areas of interest (Figure 6b). It can be seen in region 1 (Figure 6c), a nano-crystalline structure with no preferred orientation was observed with crystals in the region of 50 nm. This again was indexed at a HCP structure. In region 2 (Figure 6d), a nano-crystalline structure was also observed. This again was indexed to a HCP structure. However preferred orientation was observed. Towards the bulk of the alloy (region 3, Figure 6e) a composite electron diffraction pattern was obtained, this was could be indexed as both FCC and HCP atomic

orientations suggesting a composite diffraction signal. The formation of ε -martensite, stacking faults and shear banding was observed in the lower subsurface (>3 μm) (Figure 6f). FIB and subsequent TEM was conducted on the areas of localised debris observed on the patch area (Figure 3f). Layers in the region of 1-2 μm were observed (Figure 7). STEM-EDX analysis demonstrated that this was rich in Ti and O with traces of Cr, Fe and Al (Figure 8).

No depletion or segregation of any elemental species was seen at the interface or within the bulk material of the CoCrMo trunnion. Electron diffraction data indicates that the debris on the surface is compact and nano-crystalline nature (Figure 7c-e). Evidence of martensitic transformation and high amounts of residual strain within bulk crystals was observed directly below the transferred debris indicating high levels of strain within the microstructure.

3.1.6. TEM Analysis: Worn Surface

Typical subsurface microstructures observed in the sample taken from the highly worn regions on the CoCrMo trunnion (Figure 2, region 3) can be seen in Figure 9. A loss of the nano-crystalline layer was observed with no evidence of reformation. A bulk single crystal structure remained at the interface. Less residual strain was seen within the crystals, indicated by sharp, streak-free electron diffraction pattern. This was indexed as a typical FCC orientation found for bulk CoCrMo alloys. An interfacial layer, presumed to be Cr_2O_3, was observed and confirmed by EDX at the CoCrMo-Pt interface in the region of 3-5nm.

3.2. TMZF Taper Analysis

3.2.1. Surface deviation

Figure 10 shows the tactile CMM contour plots obtained from the TMZF taper components. Measureable material loss had occurred within the resolution of the CMM. However the depth of material loss was less compared to the CoCrMo trunnion (Figure 2). Evidence of material loss could be observed in the transverse section of the TMZF component with a maximum penetration of 14 μm being observed at ± 35-120˚ (Compared to 38 μm around ±25˚ for the CoCrMo trunnion component). The TMZF taper presented a different wear pattern with no localisation of degradation been observed when compared to the CoCrMo trunnion (Figure 2). SEM, FIB-TEM analysis was

conducted in similar regions to those described in Figure 1 in attempt to identify local degradation modes. For the reference surface, region 3 (Figure 10) was used as this provided a non-contacted blasted surface; the same found in the contacting regions.

3.2.2. SEM Analysis

Figure 11 shows the surface topographies observed on the TMZF taper component. Again, a range of topographies could be observed as a function of location. In regions where little to no degradation was observed (Figure 10, region 1 and Figure 11a) topographies were homogenous in texture and similar to those obtained through a blasting process was observed. Towards the mid portions of the interface a loss of surface topography and the presence of a surface deposit was seen (Figure 11b). Back scattered detection imaging indicated areas of deposit consisted of a lower atomic mass (ie C, Ca, P, O). Towards the distal portion of the interface, Figure 11c, a similar topography was observed to Figure 11a. A textured surface similar to that of a blasted surface was again observed. Figure 12 shows semi-quantitative SEM EDX mapping at 20 kV for the image presented in Figure 11b. Areas where a surface deposit was observed were rich in Cr, C and O. A depletion of Ti was observed in this area. No Co was observed at 20 kV. At higher magnifications, deposits were seen to be localised between the asperities of the rough surface.

Further point EDX analysis was conducted at 5 kV in order to quantify the surface chemistry of the upper most surface (≈100 nm, Figure 13). Table 1 shows the semi-quantitative values obtained from point EDX analysis at 5 kV using Lα emission lines. Across the different areas an in-homogeneous surface chemistry was observed. Surfaces were seen to be rich in C and O with Si, P and Mo observed in all areas analysed. Ti, Cr, Co and Zr were observed in spectrum 1 and 3 however Co was observed at low levels compared to the other elements.

3.2.3. XRD Analysis

Figure 14 presents the XRD plots obtained for the reference TMZF alloy and areas that had incurred highest incidences of degradation (Figure 10). For the reference TMZF surface a predominantly β-phase alloy was observed with evidence of α-phases at lower intensities. This is as expected according to literature regarding the metallurgy of the alloy [22]. Distinct difference

between the reference and degraded surface were observed. A loss of the α-Ti peaks was observed in the highly degraded regions. Significant broadening of the β-phase peaks was also observed, characteristic of an increased strain within the crystal lattice and reduction of crystal size. A gain of peaks at $2\theta \approx 46$ and 47˚ was observed. These were unidentifiable from XRD data libraries due to the lack of higher angle peaks however maybe related to the formation of Fe compounds as demonstrated later through TEM analysis. It is evident from XRD data that phase transformation and a high degree of strain is introduced into the TMZF alloy due to the degradation and plastic deformation processes occurring at the stem-neck interface.

3.2.4. TEM Analysis: Reference Surface

Figure 15 shows TEM electron micrographs of the TMZF alloy taken from manufactured surfaces which had not being subjected to any wear processes. A poly-crystalline structure was observed (white arrows indicate grain boundaries). Multiple electron diffraction micrographs of the subsurface were taken for the reference samples. Two distinctly different diffraction signals were observed. In regions 1 and 3 a ringed diffraction pattern (Figure 15) was observed. In combination with bright-field TEM images (Figure 15a) it can be seen that a two phase structure exists with β-grains containing a mixture of nano-crystalline intragranular α-precipitates. A 50 nm interfacial layer was also observed. Closer examination of the film indicated that a mixture of amorphous and crystalline material (Figure 15d).

3.2.5. TEM Analysis: Retained Patch

In the regions in which surface topography was retained on the CoCrMo trunnion component, refinement of microstructure in the bulk alloy and the formation of a metallic oxide layer could be observed on the counterpart TMZF surface (Figure 16). A nano-crystalline microstructure with preferred orientation of the crystals was observed (Figure 16a). It can be seen in Figure 16b that areas with different microstructure exist within the polycrystalline structure as highlighted by the white arrows. Precipitation and oxidation of elemental species from and within the subsurface of the TMZF alloy was confirmed with combined STEM–EDS analysis (Figure 17). In comparison with the

reference TMZF subsurface, a transformation of the subsurface microstructure and formation of metal oxides at the surface was observed.

Films consisting of metallic oxides were seen to range between 100-500 nm in thickness (Figure 16c) depending upon location. The thickest films were seen in areas around 0 degrees according to CMM contour plots (Figure 2 and 9). These were compact, crystalline and granular in nature. Films were seen to penetrate into the bulk alloy. STEM–EDX analysis (Figure 17) showed films to be Cr and O rich. Cracking of the interfacial surface and ingress of the Cr and O rich debris into the subsurface could be seen. Segregation of Fe at and below the interface was seen. The formation and propagation of subsurface cracks was also witnessed in this area (Figure 16d).

3.2.6. TEM Analysis: Worn Surface

In areas where high amounts of degradation could be observed on the CoCrMo trunnion component (Figure 2, region 3), changes in the subsurface microstructure were also observed for the counterpart TMZF surfaces. The formation of a nano-crystalline microstructure was again seen (Figure 18a and b) along with evidence of subsurface cracking and propagation.

The oxidation and segregation of species within the subsurface region of the alloy was evident. This was consistently seen up to depths of ≈ 5-10 μm. Dark-field TEM micrographs (Figure 18c and d) present evidence of nano-crystalline material, directionality and 'flow' or mechanical mixing of the TMZF alloy. STEM-EDX (Figure 19) analysis further identified the formation of oxides within the subsurface of the alloy at depths of at least 2 - 5 μm. These were Fe and O rich with depletion of Ti in the areas where iron oxides had formed. C was also found to be present and at localised regions within the subsurface of the TMZF alloy.

4. Discussion and Conclusion

Issues have surrounded bi-modular TJR since their conception; many of the initial issues concerned with fatigue and fracture were eliminated through system designs and material changes [10]. However this was a short term solution and femoral stems with exchangeable necks still have twice the rate of revision compared to fixed stems with metal related pathologies been the highest for

CoCrMo/Ti alloy combinations according to the Australian Joint Registry [23]. The nominal mode of degradation occurring at modular taper interfaces has been described extensively in the literature. It is widely accepted that a tribocorrosion degradation mechanism occur at these interfaces; coined mechanically assisted corrosion (MAC) by Gilbert *et al* [24] which also further discusses the role of possible intergranular corrosion due to the heterogeneity of metal alloys. This consists of a combination of mechanical (e.g. wear) and electrochemical (corrosion) processes resulting in accelerated degradation of the metal and release of metallic ions and debris into the biological environment. Similar observations have been identified in this study, albeit evidence of intergranular corrosion attack. Directionality of surface and evidence of mass loss was seen suggesting both corrosion and wear exist at the interface complimenting results presented by Lanting *et al* [8]. However due to the composite contact conditions established during loading (i.e. varying contact pressures and displacements across the interface), the severity and type of degradation is thought to vary across the interface as a function of contact pressure and displacement. Local variations in contact pressures and displacement will be established giving rise to very different local tribological and subsurface damage processes as discussed further below.

This study also provides insight into the underlying mechanisms contributing to the unexpectedly higher rates of degradation of CoCrMo when compared to the 'softer' titanium counter-face. This is consistent with the tactile measurements performed elsewhere [25], and supports the mesoscopic data by Buente *et al* [16], along with other retrieval studies [6]. Cook *et* al [26] presented a case of two TMZF Accolade (Stryker, Warsaw, USA) stems used in conjunction with CoCrMo femoral heads. They hypothesised that the TMZF alloy, due to its increased nobility, cathodically protected itself at the expense of the CoCMo alloy accelerating the degradation of the CoCrMo component. Similar observations have been seen in other device combinations [27].

Whilst counter intuitive of most engineering tribology theory, this has also been attributed to a tribocorrosion mechanism; owing to the formation of thick and hard surface oxides and subsequent abrasion of the CoCrMo surface [28]. Findings presented in this paper support these theories in part. Whilst small mass losses and negligible changes to topography may occur on the Ti alloy

surface, subsurface analysis suggest plastic flow of material, gross straining, refinement of microstructure and 'mechanical alloying' process; the extent of which varies dependent upon the region within the interface. The importance of subsurface and interfacial microstructure has been well documented in the orthopaedic sector [29,30]. Many authors have presented evidence of dynamic recrystallization [31], strain-induced transformation and the formation of nano-crystalline material of CoCrMo articulating surfaces in both retrieval and experimental studies [32]. However these have mainly been concerned with reciprocating hard-on-hard surfaces of which are now almost obsolete. It has been hypothesised that shear stresses present during sliding results in the formation of nano-crystalline layers at the upper most surface of the material. These have been associated with an increase in interfacial hardness and the origin of nano-scale debris typically associated with Metal-on-Metal bearings [33,34]. Furthermore the changes in subsurface microstructure and tribo-chemical processes (chemical reactions owing to the tribological interactions) have been hypothesised to contribute to the overall degradation of sliding interfaces [35-37]. Zeng *et al* [32] has recently demonstrated decreases in wear depending upon the initial interfacial crystallinity. Whilst the evolution mechanisms for microstructural changes appear to be strain dependant and similar regardless of the initial crystallinity, clinical findings do not correlate in the case for fretting contacts.

Mathew *et al* [35] has recently shown the effect of SIT on the corrosion response of CoCrMo supporting findings by Montero-Ocampo *et al* [38]. It has been shown that HC CoCrMo alloys possess lower passive corrosion currents when in bulk like FCC form. Whilst a wealth of knowledge exists for sliding interfaces, in which the tribology has been refined over a number of years, only one study deals with the processes occurring at the nano-scale for modular taper surface [39] (either stem-neck or head-neck). This is surprising considering the breadth of research currently been conducted in this area.

For the CoCrMo trunnion component, changes in subsurface morphology incurred during implantation can be summarised as follows (Figure 20):

- In the regions where high contact pressures exist (ie patch areas) [8,40-42], little changes to the topography could be seen. However subsurface analysis (Figure 6) revealed evidence of martensitic transformation processes, shear material and higher strain within the CoCrMo lattice when compared to the reference sample (Figure 5). The retention of topography similar to that of unworn areas in this area may suggest evidence of a 'stick' fretting regime in which no relative micro-motion occurs at the interface. For elastic fretting couples such as (CoC-Ti alloys) the elasticity of the Ti alloy will dominate and slip at the interface will be accommodated by nominal elastic deformation of the bodies [41]. Swaminathan and Gilbert [42] suggest within these regimes, tribocorrosion contributions to mass low tend to be low as abrasion of the oxide film does not occur. Evidence of galling and transfer of TMZF alloy to the CoCrMo patch area was observed (Figure 8). Layers composed of Ti and O with evidence of oxidation of other species within the films suggests that such layers may be formed due to fatigue and transfer of the TMZF to the CoCrMo surface during daily loading activity rather than during disassembly. If transfer of material occurred during dis-assembly it would be expected that this would be bulk material. EDX analysis (Figure 7) demonstrates this is not the case. Transfer of oxidised material is extensively reported in classic fretting data of elastic differential alloy systems [43,41,44].
- TEM analysis in highly degraded region demonstrated a different subsurface response. A loss of the manufactured induce nano-crystalline layer was observed resulting in a single crystal FCC being observed at the interface (Figure 9). Although difficult to quantify from retrieval analysis which only presents one point in time, loss of any nano-crystalline layers may occur as a result of mechanical and electrochemical processes. For this particular contact, electrochemical reactions could become dominant as the crevice depth becomes sufficiently deep enough so mechanical deformations are insufficient to result in metal-metal contact, mechanical material removal and further subsurface microstructural changes. Acidification of the solution at the interface is likely to occur increasing rates of dissolution due to localised crevice corrosion. Such

phenomenon has already been reported by Bryant et al [20] for the stem-cement interface. Further research into understanding these mechanisms is needed.

To the authors knowledge the interactions between fretting-corrosion, subsurface damage mechanisms and 'mechanical alloying' processes observed on the TMZF alloy have not yet been reported. Considering the current debate as to why CoCrMo alloys degrade compared to the softer titanium alloy when used in a modular taper arrangement, results presented in this paper present a new hypothesis concerning the mechanisms acting at the modular-taper interface. Evidence of the formation of tribo-materials (i.e. a material formed as a result of tribology), fatigue of the TMZF (i.e. crack initiation and propagation), plasticity (i.e. permanent change in subsurface morphology) and oxidation and the formation of new phases at the interface is shown in Figure 16 and 18.

The formation of tribomaterial consisting of nano-crystalline material and discreet oxide phases within the subsurface material presents a fascinating system characteristic; raising questions as to how the initiation and propagation of wear and corrosion at the modular interface will be effected. β-titanium alloys are known to show improvement in their wear resistance due to their ability to facilitate strain hardening and microstructure refinement, assumable through a martensitic transformation mechanism. In a review by Long and Rack [22], they highlighted that sub-surface wear damage of cp-Ti has been investigated with cross sections of wear samples revealing a layer of compacted debris at the worn surface, with plastic flow of the material beneath. Refinement, transformation of the TMZF microstructure and the formation of oxide phases within the subsurface material, hypothesised as a result of cyclic loading, fatigue and corrosion, was observed in this study. Consequently a material whose interfacial properties that are very different to their bulk mechanical properties will be generated, effecting the wear and corrosion processes occurring at the interface. The formation of iron oxides, thought to arise from an ingress of fluid and oxidation of bulk material, also shows that the interfacial chemistry is also affected by a combined mechanical and electrochemical process. The oxidation of iron is not surprising considering its thermodynamic tendency for oxidation [45]. However the standard cell potentials (E_o) for the species present in the alloy are not signifanlty more negative than Ti, Mo and Zr; hence thermodynamic principles cannot

be solely applied to this situation. This now raises question around the kinetic of the reaction processes and how external factors, such as stress, occurring at the surface and subsurface influence the formation of these species.

Whilst the exact mechanisms and rates of degradation cannot be determined in this study, an insight into the mechanisms behind high rates of wear and corrosion of CoCrMo surfaces when used in conjunction with a Ti alloy counter-face can be gained. Figure 20 shows a schematic of the CoCrMo and TMZF subsurface based on location analysed. A composite material with an increased interfacial hardness and different surface chemistry when compared to the bulk is likely to form as a result of initial degradation within the interface. Literature reports some iron oxides to have a hardness in the region of > 5 GPa depending upon their nature; similar to the hardness of the CoCrMo alloy. It is quite credible that the combination of a refined microstructure, formation of oxide phases and in increase in residual stress within the alloy subsurface may result in a material surface capable of inducing higher wear and corrosion on the CoCrMo surface. Furthermore taking into account the fact that in highly worn regions of the CoCrMo a bulk single crystal FCC structure was observed, the hardness at the interface may be less making it more susceptible to wear processes. Galvanic interactions at the interface between the mixed metals may also contribute to the accelerated degradation of the CoCrMo alloy due to potential differences established by each material. However due to the nature of the interface this almost impossible to quantitatively assess this; further experimental work utilising novel contact arrangements will be developed to simulate this *in-vitro.*

4.1. Limitations of Study

This study presents the in-depth analysis of a single implant as part of a retrieval series presented by Buente et al [16]. As such, this study is limited to a single case. None the less provides important information about interfacial processes occurring at CoCrMo-TMZF fretting interfaces as a function of interfacial contact conditions. The finding presented demonstrate the synergy and interaction between the two material when in contact *in-vivo* and the subsequent evolution of subsurface microstructure and surface chemistry. Further work will involve the observation of further *in-vivo*

combinations and experimental investigation to determine the system variables and mechanisms behind the observations reported in this study.

5. Conclusions

From this study, it is evident that complex and synergistic degradation processes are occurring at stem-neck interface of bi-modular prosthesis. This consists of mechanical and electrochemical processes resulting in changes to interfacial properties of the materials.

Detailed electron microscopy, has highlighted that the extent and type of degradation occurring at the interface depends upon the local mechanical contact conditions with difference in subsurface morphology and chemistry been observed at different points across the interface. In regions where high stress are established, retention of the initial topography and evidence of plastic deformation of the bulk material suggests that whilst no macroscopic topographical degradation is occurring, permeant subsurface changes have occurred.

An further hypothesis as to why CoCrMo alloys experience higher rates of mass loss compared to the Ti alloy surface when used in modular taper contacts is also presented. Higher degradation of the CoCrMo alloy surface may arise from an increase in interfacial hardness of the TMZF alloy due to refinement of the subsurface microstructure and formation of oxides species at the interface. Further systematic, spatially resolved experimental studies are needed to identify the underlying mechanisms to progress the current understanding.

References

1. Collier, J., Surprenant, V., Jensen, R., Mayor, M., Surprenant, S.: Corrosion between the components of modular femoral hip prostheses. Journal of bone and joint surgery [Br] **74-B**, 511-517 (1992).
2. Goldberg, J., Gilbert, J.: Electrochemical responce of CoCrMo to high-speed fracture of its metal oxide using an electrochemical scratch test method. J Biomed Res **37**, 421-431 (1997).
3. Goldberg, L., Gilbert, J.: *In Vitro* Corrosion Testing of Modular Hip Tapers. J Biomed Mater Res Part B **64B**, 79-93 (2003).
4. Panagiotidou, A., Meswania, J., Osman, K., Bolland, B., Latham, J., Skinner, J., Haddad, F.S., Hart, A., Blunn, G.: The effect of frictional torque and bending moment on

corrosion at the taper interface: An in vitro study. Bone and Joint Journal **97-B**(4), 463-472 (2015). doi:10.1302/0301-620X.97B4.34800

5. Bolland, B.J.R.F., Culliford, D.J., Langton, D.J., Millington, J.P.S., Arden, N.K., Latham, J.M.: High failure rates with a large-diameter hybrid metal-on-metal total hip replacement: clinical, radiological and retrieval analysis. Journal of Bone & Joint Surgery, British Volume **93-B**(5), 608-615 (2011). doi:10.1302/0301-620x.93b5.26309

6. Hothi, H.S., Matthies, A.K., Berber, R., Whittaker, R.K., Skinner, J.A., Hart, A.J.: The Reliability of a Scoring System for Corrosion and Fretting, and Its Relationship to Material Loss of Tapered, Modular Junctions of Retrieved Hip Implants. The Journal of Arthroplasty **29**(6), 1313-1317 (2014). doi:http://dx.doi.org/10.1016/j.arth.2013.12.003

7. Baxmann, M., Jauch, S.Y., Schilling, C., Blömer, W., Grupp, T.M., Morlock, M.M.: The influence of contact conditions and micromotions on the fretting behavior of modular titanium alloy taper connections. Medical Engineering & Physics **35**(5), 676-683 (2013). doi:http://dx.doi.org/10.1016/j.medengphy.2012.07.013

8. Lanting, B.A., Teeter, M.G., Vasarhelyi, E.M., Ivanov, T.G., Howard, J.L., Naudie, D.D.R.: Correlation of Corrosion and Biomechanics in the Retrieval of a Single Modular Neck Total Hip Arthroplasty Design: Modular Neck Total Hip Arthroplasty System. The Journal of Arthroplasty **30**(1), 135-140 (2015). doi:http://dx.doi.org/10.1016/j.arth.2014.06.009

9. Hermle, T., Zeller, R., Grupp, T., Blomer, W.: Metha short stem hip prosthesis - Examination of the modular cone connection. (1/07), 12 - 17 (2007).

10. Grupp, T., Weik, T., Bloemer, W., Knaebel, H.-P.: Modular titanium alloy neck adapter failures in hip replacement - failure mode analysis and influence of implant material. BMC Musculoskeletal Disorders **11**(1), 3 (2010).

11. Orthopeadics, S.: Rejuvenate Modular / ABG II Modular-Neck Stem Voluntary Recall. (2014). Accessed 13/11/2015 2015

12. Barlow, B.T., Assini, J., Boles, J., Lee, Y.Y., Westrich, G.H.: Short-Term Metal Ion Trends Following Removal of Recalled Modular Neck Femoral Stems. Journal of Arthroplasty **30**(7), 1191-1196 (2015). doi:10.1016/j.arth.2015.02.033

13. De Martino, I., Assini, J.B., Elpers, M.E., Wright, T.M., Westrich, G.H.: Corrosion and Fretting of a Modular Hip System: A Retrieval Analysis of 60 Rejuvenate Stems. Journal of Arthroplasty **30**(8), 1470-1475 (2015). doi:10.1016/j.arth.2015.03.010

14. Kao, C., Scalettar, R., Bunning, R.D.: Two Cases of Metallosis from Metal-on-Polyethylene Total Hips: AnEmerging Problem. PM and R **7**(4), 447-450 (2015). doi:10.1016/j.pmrj.2014.11.004

15. Meftah, M., Haleem, A.M., Burn, M.B., Smith, K.M., Incavo, S.J.: Early corrosion-related failure of the Rejuvenate modular total hip replacement. Journal of Bone and Joint Surgery - Series A **96**(6), 481-487 (2014). doi:10.2106/JBJS.M.00979

16. Buente, D., Huber, G., Bishop, N., Morlock, M.: Quantification of material loss from the neck piece taper junctions of a bimodular primary hip prosthesis. A retrieval study from 27 failed Rejuvenate bimodular hip arthroplasties. Bone & Joint Journal **97-B**(10), 1350-1357 (2015). doi:10.1302/0301-620x.97b10.35342

17. Witt, F., Gührs, J., Morlock, M.M., Bishop, N.E.: Quantification of the contact area at the head-stem taper interface of modular hip prostheses. PLoS ONE **10**(8) (2015). doi:10.1371/journal.pone.0135517

18. Rehmer, A., Bishop, N.E., Morlock, M.M.: Influence of assembly procedure and material combination on the strength of the taper connection at the head-neck junction of modular hip endoprostheses. Clinical Biomechanics **27**(1), 77-83 (2012). doi:10.1016/j.clinbiomech.2011.08.002

19. Goldberg, J., Gilbert, J., Jacobs, J., Bauer, T., Paprosky, W., Leurgans, S.: A multicenter retrieval study of the taper interfaces of modular hip prostheses. Clin Orth Rel Res(401), 149 - 161 (2002).

20. Bryant, M., Farrar, R., Freeman, R., Brummitt, K., Neville, A.: Fretting corrosion characteristics of polished collarless tapered stems in a simulated biological environment. Tribology International **65**(0), 105-112 (2013).

21. Vingsbo, O., Schön, J.: Wear of Materials: Proceedings of the 9th International Conference Gross slip criteria in fretting. Wear **162**, 347-356 (1993). doi:http://dx.doi.org/10.1016/0043-1648(93)90518-Q

22. Long, M., Rack, H.J.: Titanium alloys in total joint replacement—a materials science perspective. Biomaterials **19**(18), 1621-1639 (1998). doi:http://dx.doi.org/10.1016/S0142-9612(97)00146-4

23. Austrailian orthopeadic association: National Joint Replacement Registry - ANNUAL REPORT. In. (2015)

24. Gilbert, J.L., Buckley, C.A., Jacobs, J.J.: In vivo corrosion of modular hip prosthesis components in mixed and similar metal combinations. The effect of crevice, stress, motion, and alloy coupling. Journal of Biomedical Materials Research **27**(12), 1533-1544 (1993). doi:10.1002/jbm.820271210

25. Langton, D.J., Sidaginamale, R., Lord, J.K., Nargol, A.V.F., Joyce, T.J.: Taper junction failure in large-diameter metal-on-metal bearings. Bone and Joint Research **1**(4), 56-63 (2012). doi:10.1302/2046-3758.14.2000047

26. Cook, R.B., Bolland, B.J.R.F., Wharton, J.A., Tilley, S., Latham, J.M., Wood, R.J.K.: Pseudotumour Formation Due to Tribocorrosion at the Taper Interface of Large Diameter Metal on Polymer Modular Total Hip Replacements. The Journal of Arthroplasty **28**(8), 1430-1436 (2013). doi:http://dx.doi.org/10.1016/j.arth.2013.02.009

27. Kiran, M., Boscainos, P.J.: Adverse Reactions to Metal Debris in Metal-On-Polyethylene Total Hip Arthroplasty Using a Titanium-Molybdenum-Zirconium-Iron Alloy Stem. The Journal of Arthroplasty **30**(2), 277-281 (2015). doi:http://dx.doi.org/10.1016/j.arth.2014.06.030

28. Moharrami, N., Langton, D.J., Sayginer, O., Bull, S.J.: Why does titanium alloy wear cobalt chrome alloy despite lower bulk hardness: A nanoindentation study? Thin Solid Films **549**, 79-86 (2013). doi:http://dx.doi.org/10.1016/j.tsf.2013.06.020

29. Pourzal, R., Theissmann, R., Morlock, M., Fischer, A.: Micro-structural alterations within different areas of articulating surfaces of a metal-on-metal hip resurfacing system. Wear **267**, 689-694 (2009).

30. Fischer, A., Weiss, S., Wimmer, M.: The Tribologocal Difference Between Biomedical Steels and CoCrMo-alloys. Jorunal of Mechanical Behaviour of Biomedical Materials **9**, 50-62 (2012).

31. Rainforth, W.M., Zeng, P., Ma, L., Valdez, A.N., Stewart, T.: Dynamic surface microstructural changes during tribological contact that determine the wear behaviour of hip prostheses: Metals and ceramics. Faraday Discussions **156**, 41-57 (2012). doi:10.1039/c2fd00002d

32. Zeng, P., Rana, A., Thompson, R., Rainforth, W.M.: Subsurface characterisation of wear on mechanically polished and electro-polished biomedical grade CoCrMo. Wear **332–333**, 650-661 (2015). doi:http://dx.doi.org/10.1016/j.wear.2015.02.007

33. Wimmer, M.A., Sprecher, C., Hauert, R., T+ñger, G., Fischer, A.: Tribochemical reaction on metal-on-metal hip joint bearings: A comparison between in-vitro and in-vivo results. Wear **255**, 1007-1014 (2003). doi:doi: 10.1016/S0043-1648(03)00127-3

34. Liao, Y., Hoffman, E., Wimmer, M.A., Fischer, A., Jacobs, J.J., Marks, L.D.: CoCrMo Metal-on-metal hip replacements. Phys.Chem.Chem.Phys. **15**, 746-756 (2013).

35. Mathew, M.T., Nagelli, C., Pourzal, R., Fischer, A., Laurent, M.P., Jacobs, J.J., Wimmer, M.A.: Tribolayer formation in a metal-on-metal (MoM) hip joint: An electrochemical investigation. Journal of the Mechanical Behavior of Biomedical Materials **29**, 199-212 (2014). doi:http://dx.doi.org/10.1016/j.jmbbm.2013.08.018

36. Hesketh, J., Ward, M., Dowson, D., Neville, A.: The composition of tribofilms produced on metal-on-metal hip bearings. Biomaterials **35**(7), 2113-2119 (2014). doi:http://dx.doi.org/10.1016/j.biomaterials.2013.11.065

37. M.Bryant, R.Farrar, R.Freeman, K.Brummitt, J.Nolan, A.Neville: Failure analysis of cemented metal-on-metal total hip replacements from a single centre cohort. http://dx.doi.org/10.1016/j.wear.2012.12.013i (2013).

38. Montero-Ocampo, C., Juarez, R., Salinas-Rodriguez, A.: Effect of Fcc-Hcp Phase Transformation Produced by Isothermal Aging on the Corrosion Resistance of a Co-27Cr-5Mo-0.05C Alloy. METALLURGICAL AND MATERIALS TRANSACTIONS A **33** (2002).

39. Zeng, P., Rainforth, W.M., Cook, R.B.: Characterisation of the oxide film on the taper interface from retrieved large diameter metal on polymer modular total hip replacements. Tribology International **89**, 86-96 (2015). doi:http://dx.doi.org/10.1016/j.triboint.2014.12.012

40. Gill, I.P.S., Webb, J., Sloan, K., Beaver, R.J.: Corrosion at the neck-stem junction as a cause of metal ion release and pseudotumour formation. Journal of Bone & Joint Surgery, British Volume **94-B**(7), 895-900 (2012). doi:10.1302/0301-620x.94b7.29122

41. Oladokun, A., Pettersson, M., Bryant, M., Engqvist, H., Persson, C., Hall, R., Neville, A.: Fretting of CoCrMo and Ti6Al4V alloys in modular prostheses. Tribology - Materials, Surfaces & Interfaces **0**(0), 1751584X1751515Y.0000000014. doi:doi:10.1179/1751584X15Y.0000000014

42. Swaminathan, V., Gilbert, J.L.: Fretting corrosion of CoCrMo and Ti6Al4V interfaces. Biomaterials **33**(22), 5487-5503 (2012). doi:http://dx.doi.org/10.1016/j.biomaterials.2012.04.015

43. Waterhouse, R.B.: Fretting Corrosion. International series of monographs on materials science and technology, Pergamon press, Cambridge, UK, (1972)

44. Budinski, K.G.: Tribological properties of titanium alloys. Wear **151**(2), 203-217 (1991). doi:http://dx.doi.org/10.1016/0043-1648(91)90249-T

45. Fontanna, M.: Corrosion Engineering, vol. 1, 3 ed. McGraw-Hill Series in Materials Science & Engineering. McGraw-Hill Book Company, (1985)

Acknowledgements

The research has received funding from the European Union's Seventh Framework Program (FP7/2007-2013) under grant agreement no. GA-310477 (Life- LongJoints).

List of Figures

Figure 14 – XRD spectra for reference and degraded areas of TMZF alloy

Figure 15 – a) Reference TEM images for TMZF Taper component with typical diffraction pattern from region b) 1 c) and 2. Figure 10d shows evidence of a films formed on the TMZF surface with possible short range ordering.

Figure 16 –a) Bright field image with associated bulk electron diffraction pattern demonstrating TMZF reorientation and oxide layer formation (white arrows indicate layer) b) a dark-field image of TMZF alloy in the patch area showing evidence of local deviations in atomic ordering within the bulk alloy (shown by white arrows). Figure 10c represents bright-field images of debris on the surface and d) evidence of subsurface fatigue and cracking (indicated by arrows).

Figure 17 – STEM-EDX analysis of and subsurface microstructure of TMZF alloy in the patch region 2 on Figure 2.

Figure 18 – An a) overview with associated bulk electron diffraction pattern b) magnification of the interface and evidence of subsurface defects c-d) dark-field images and evidence of re-crystallisation and mechanical mixing with the subsurface microstructure of TMZF alloy in highly degraded areas (Figure 1, region 3).

Figure 19 - STEM-EDX analysis of and subsurface microstructure of TMZF alloy in the highly degraded region.

Figure 20 – illustration of the subsurface morphology for CoCrMo taper and TMZF trunnion in each of the regions analysed.

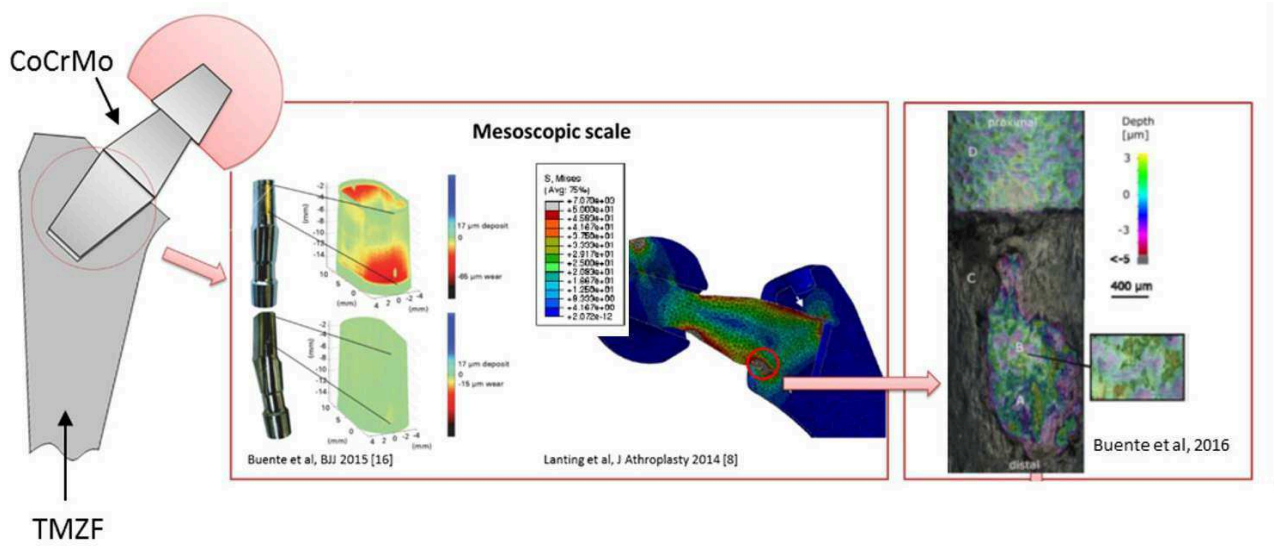

Figure 1

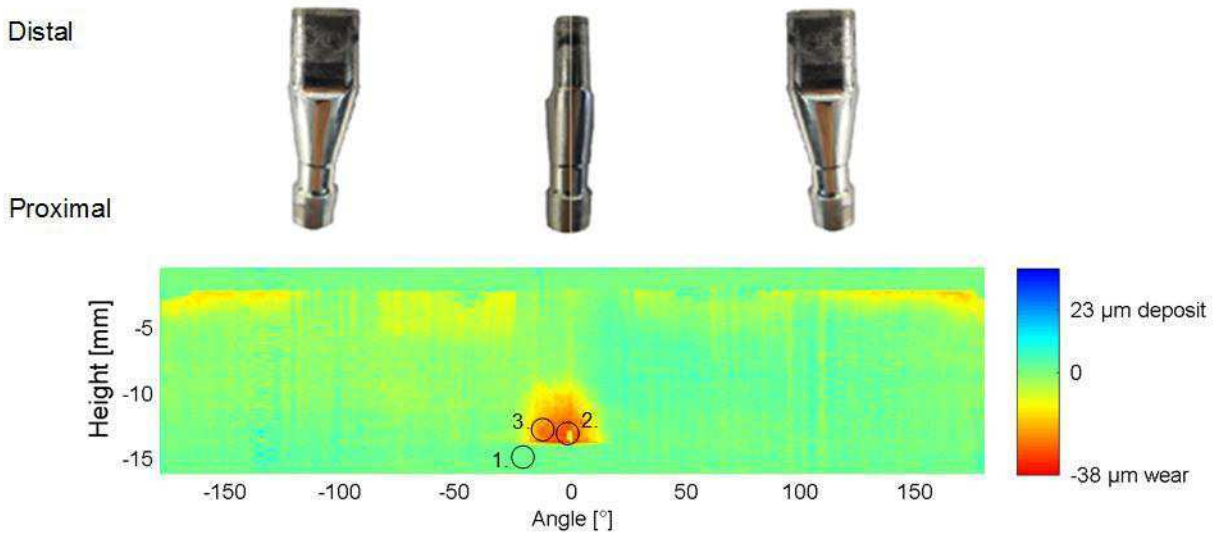

Figure 2

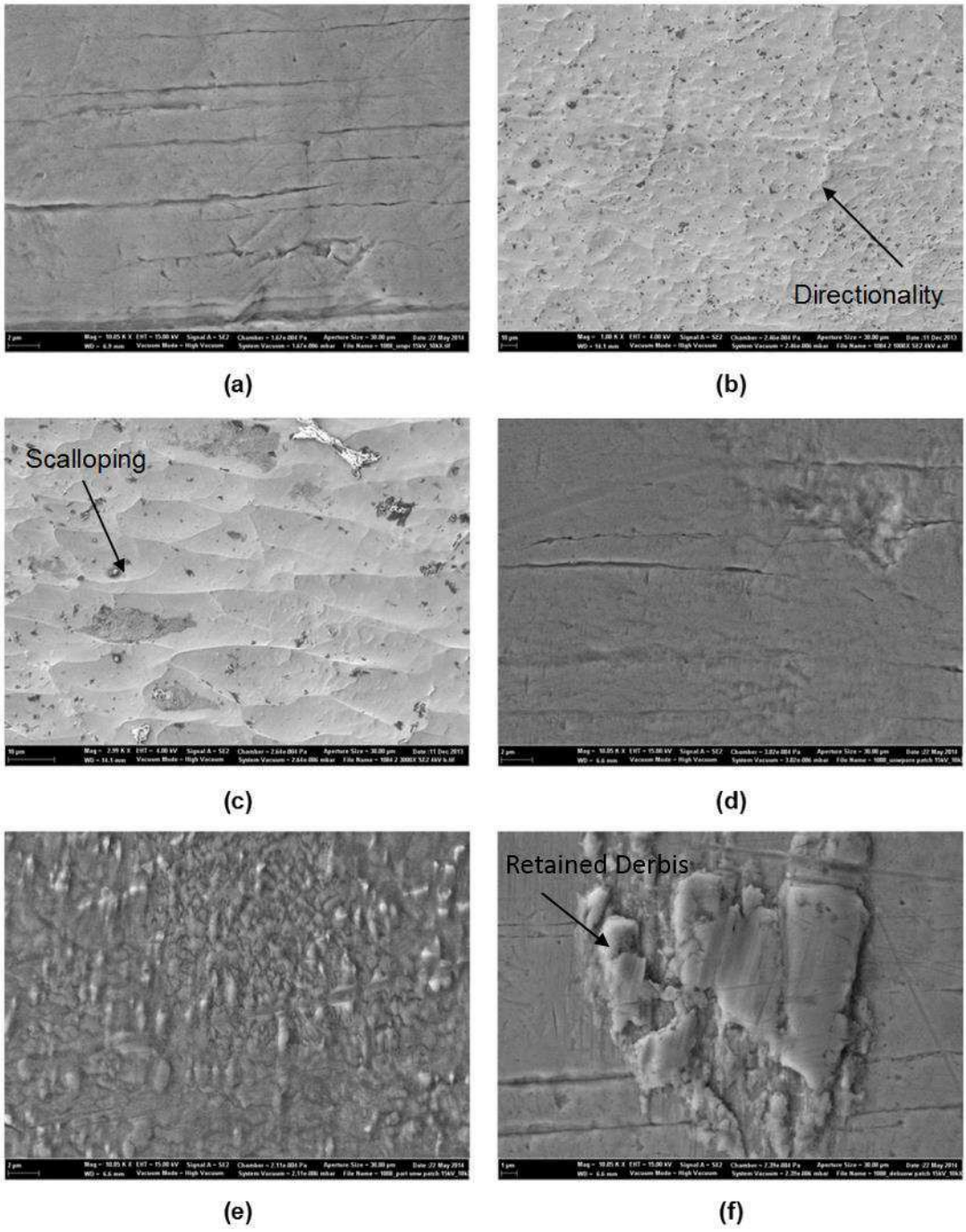

Figure 3

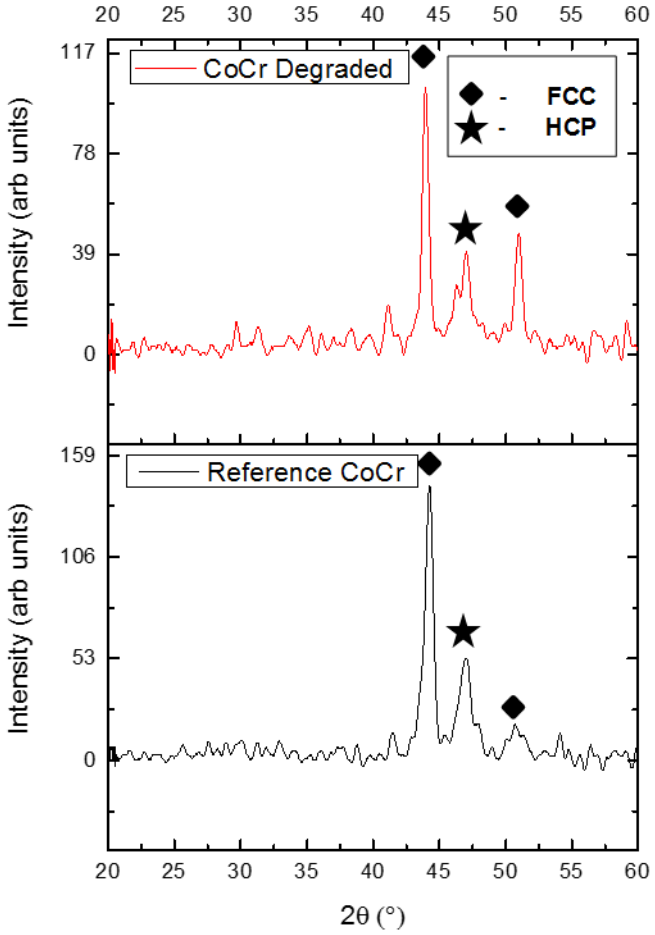

Figure 4

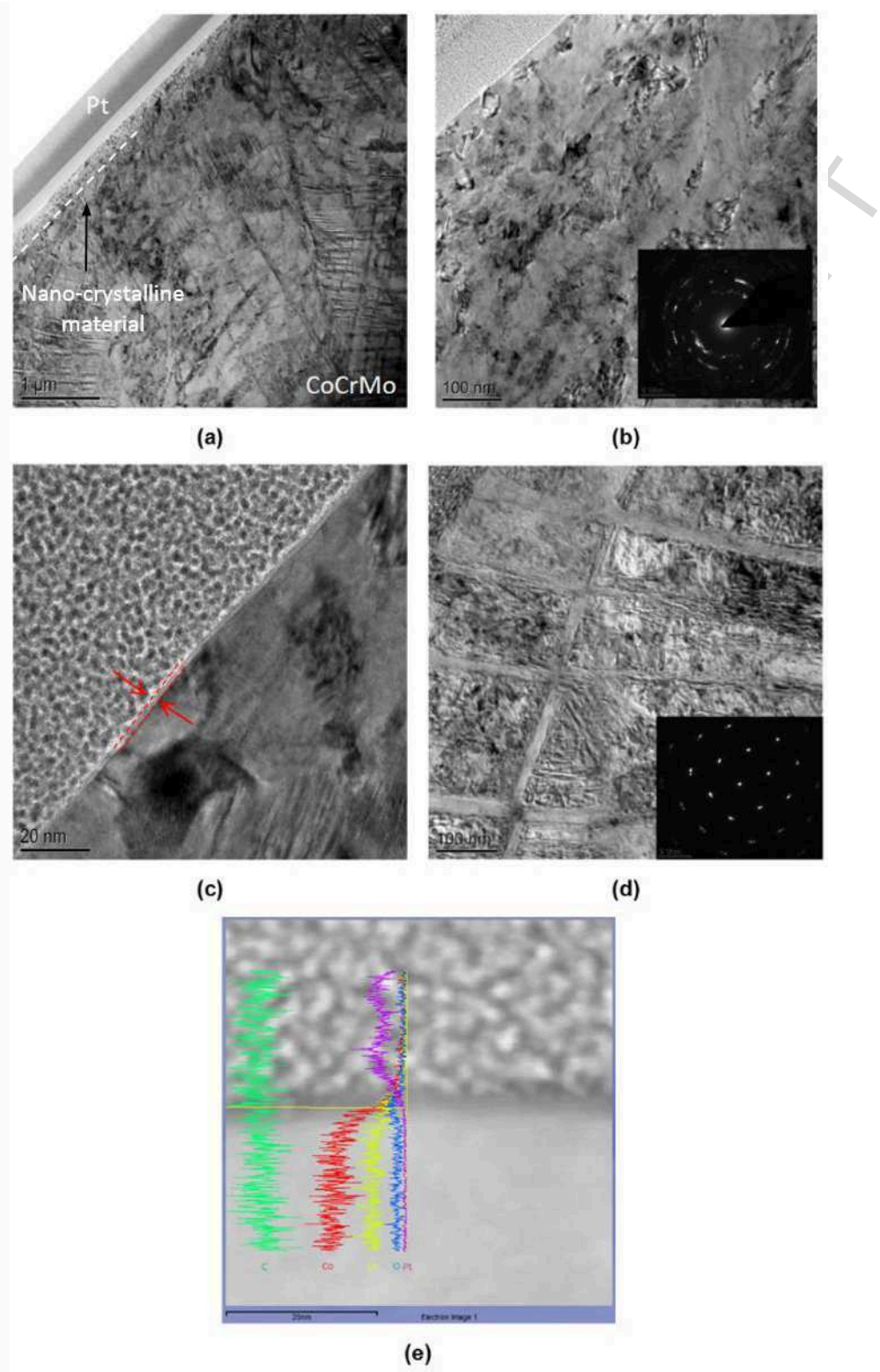
Pt
Nano-crystalline material
1 μm
CoCrMo
(a)
100 nm
(b)
20 nm
(c)
100 nm
(d)
(e)

Figure 5

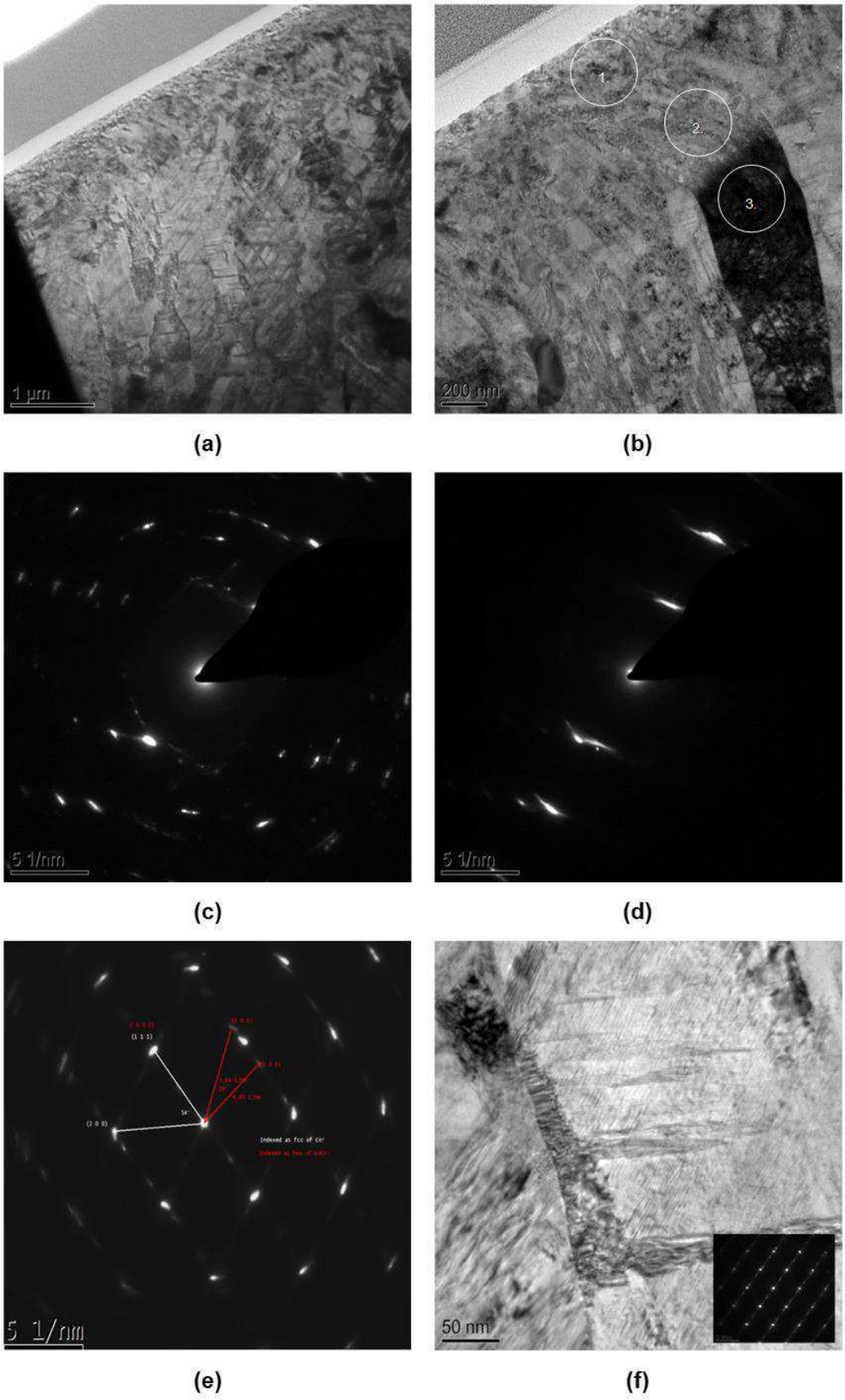

Figure 6

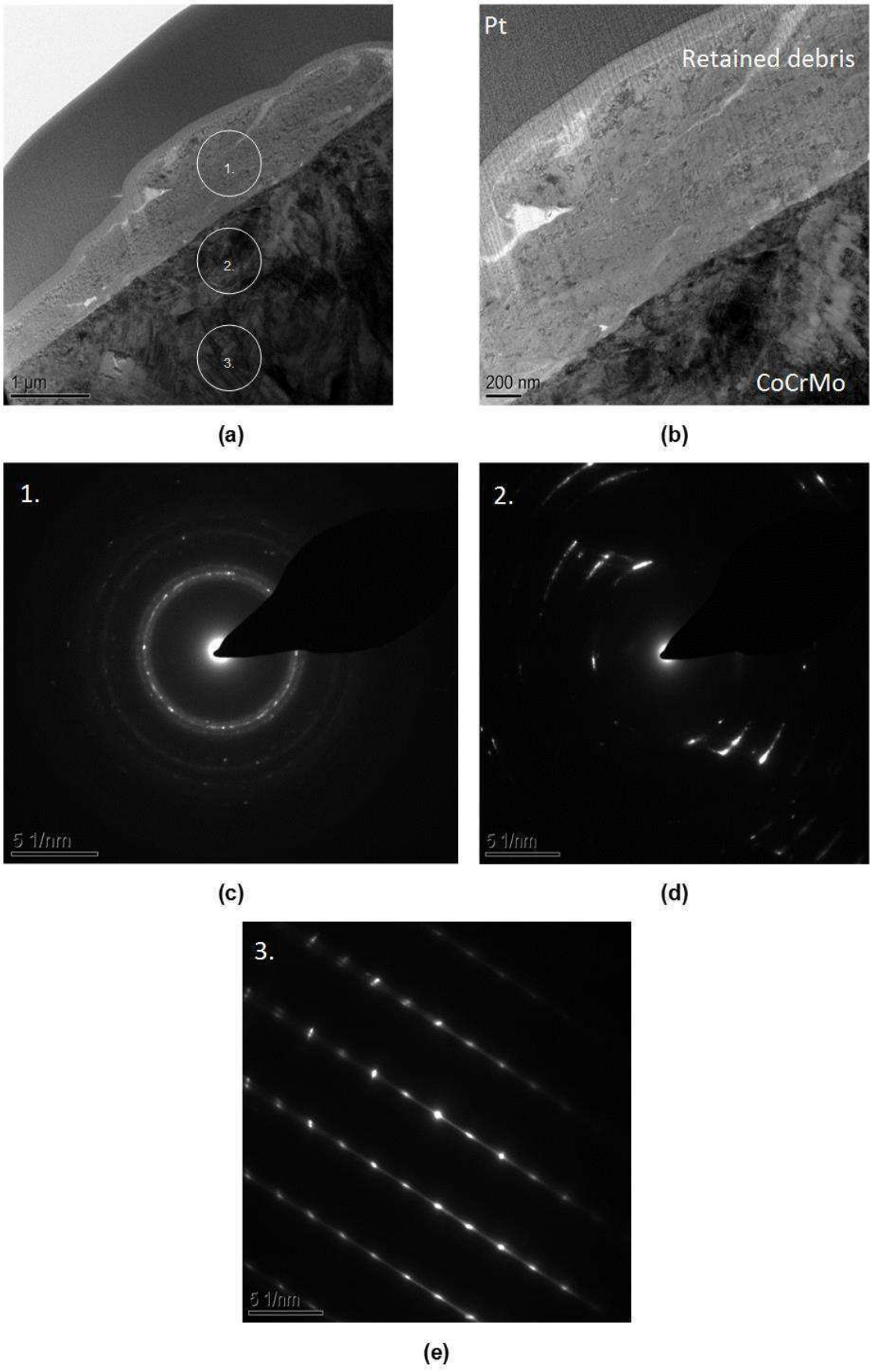
1.
2.
3.
1 µm
(a)
Pt
Retained debris
200 nm
CoCrMo
(b)
1.
5 1/nm
(c)
2.
5 1/nm
(d)
3.
5 1/nm
(e)

Figure 7

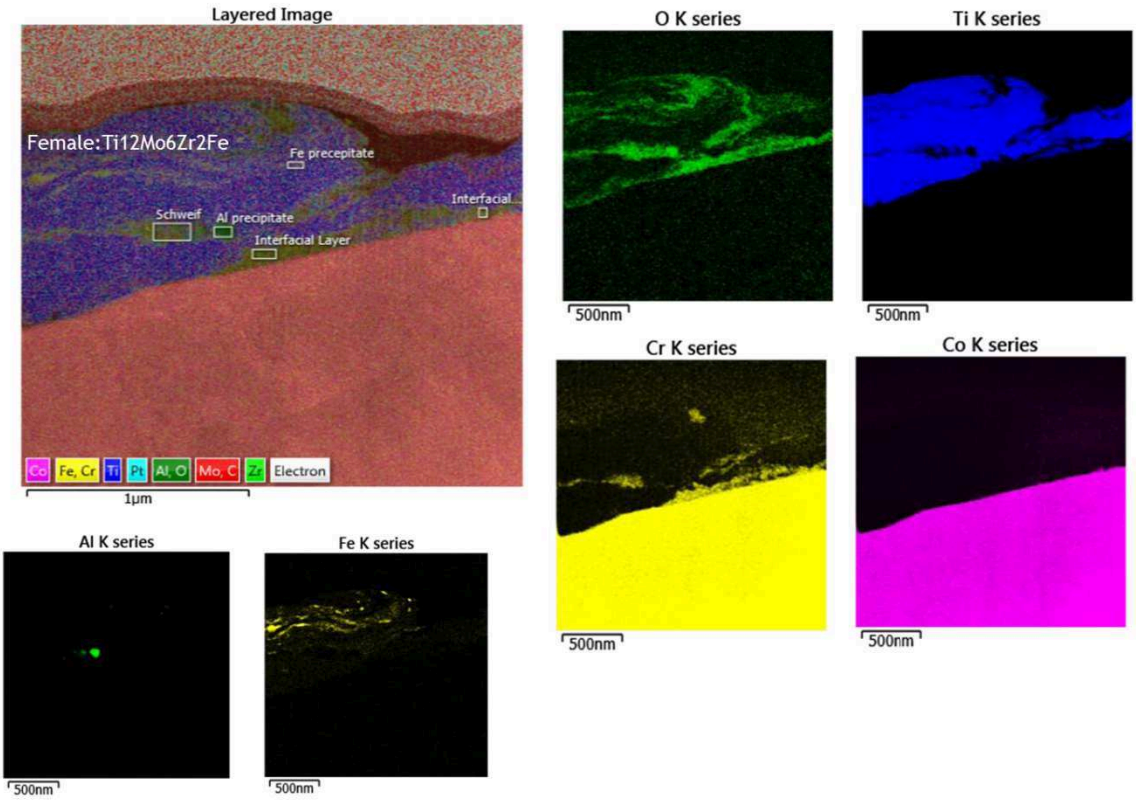

Figure 8

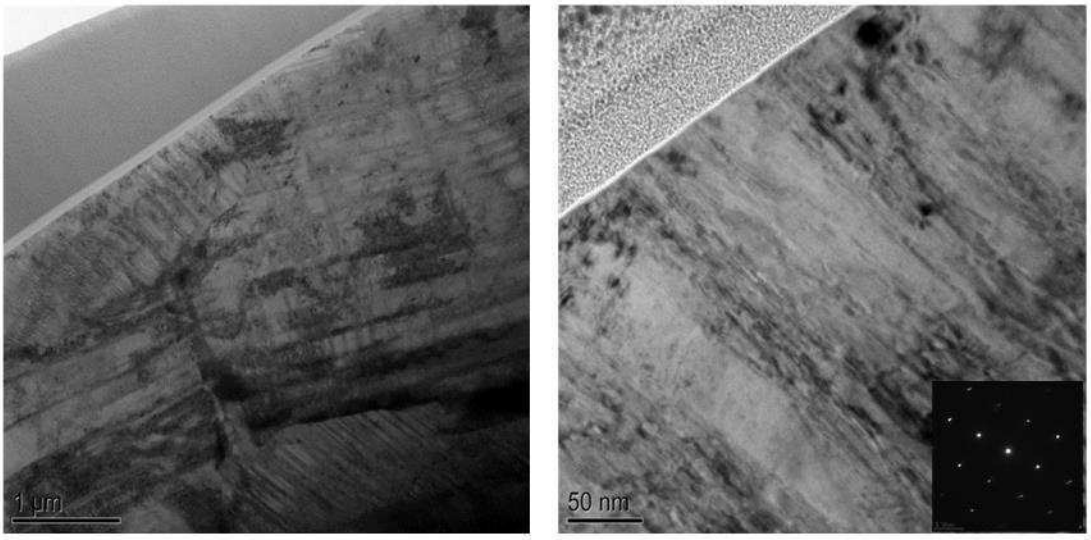

Figure 9

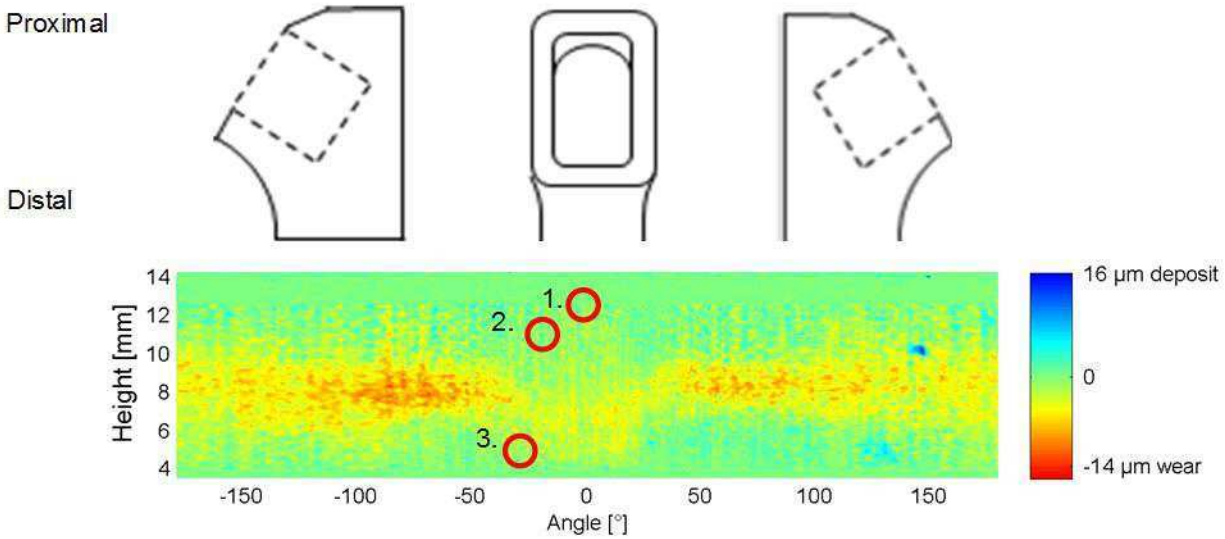

Figure 10

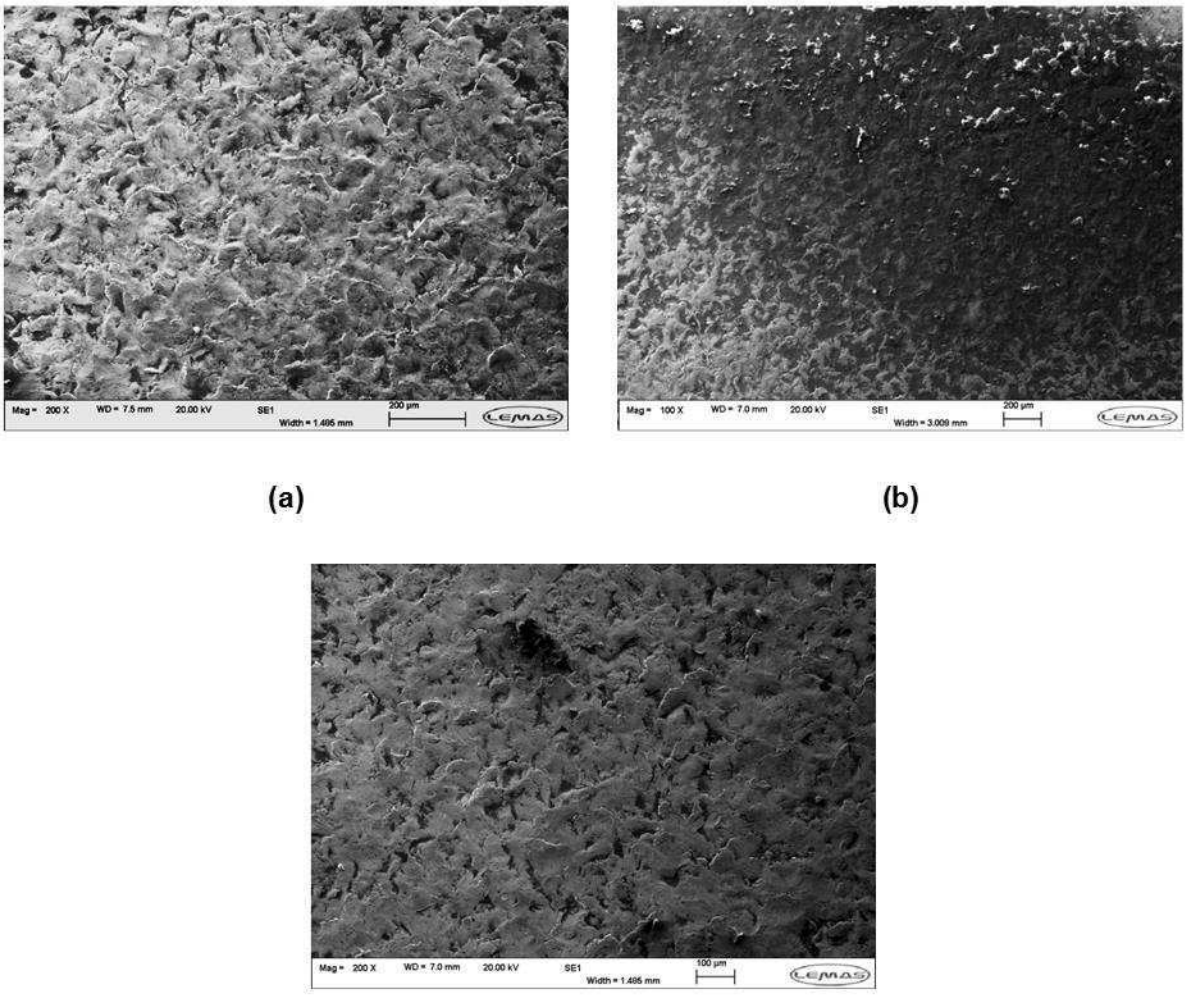

Figure 11

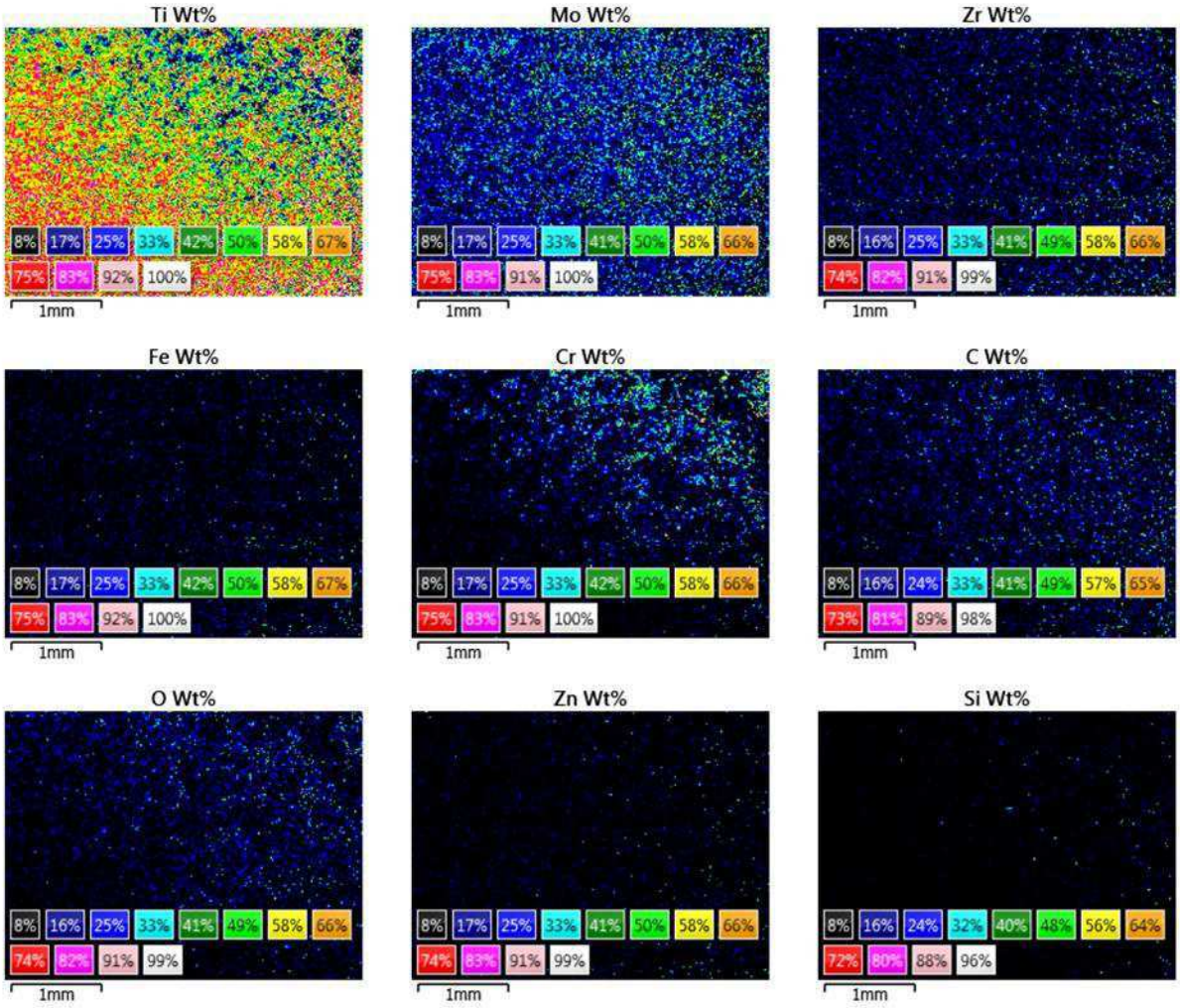

Figure 12

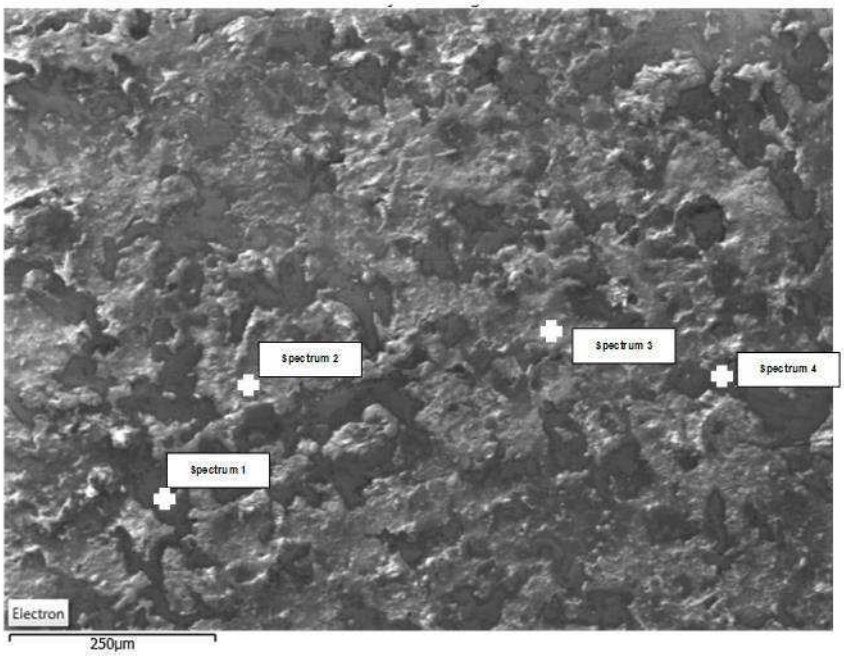

Figure 13

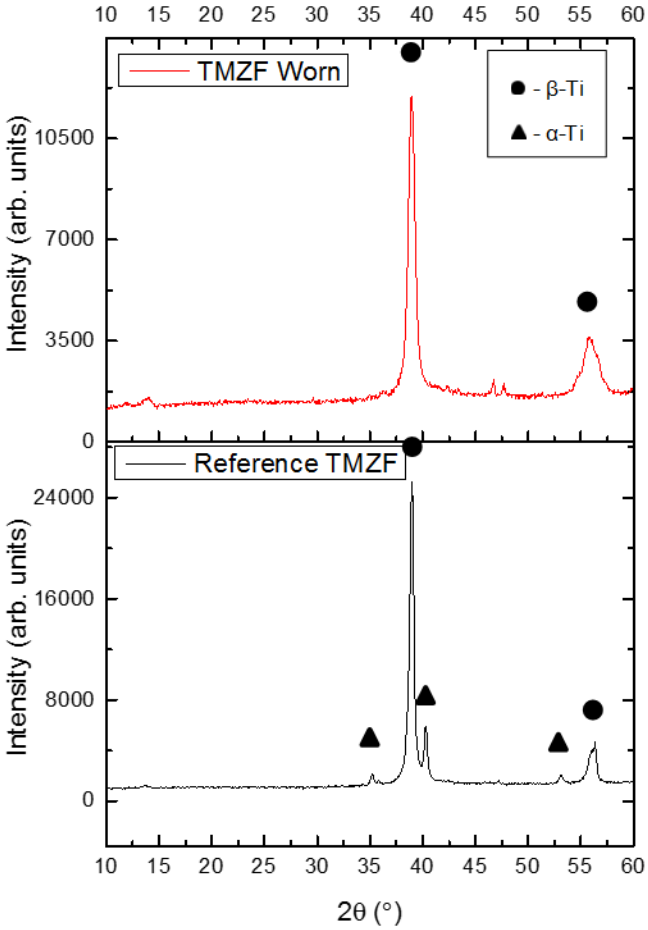

Figure 14

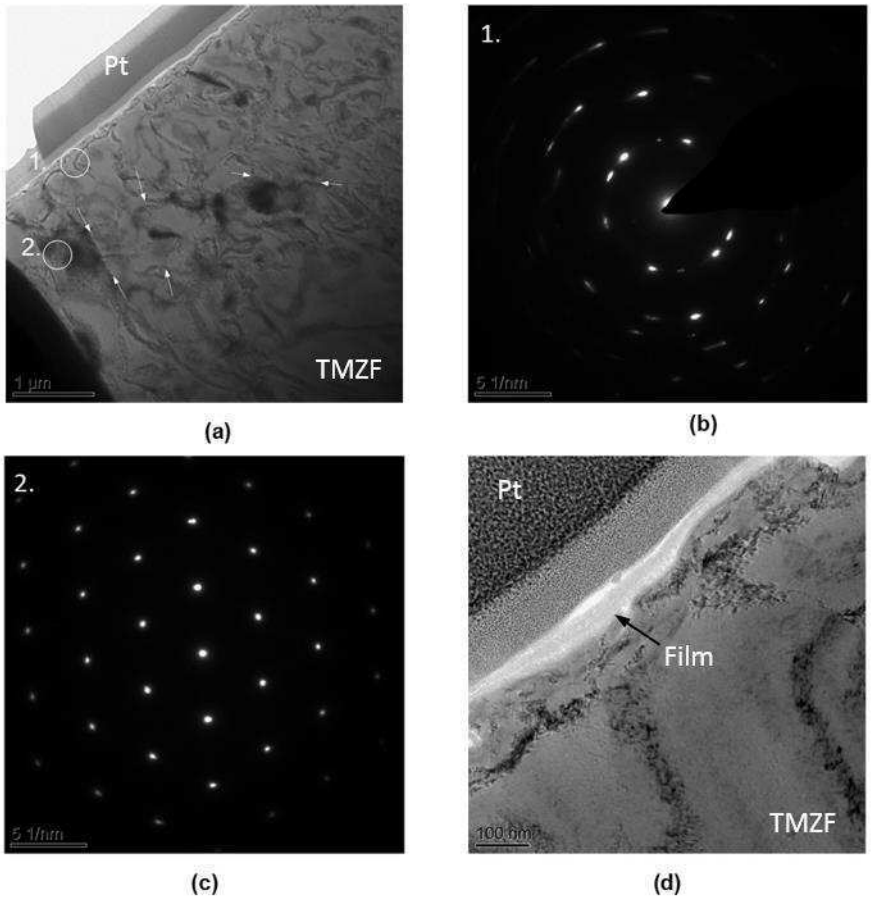

Figure 15

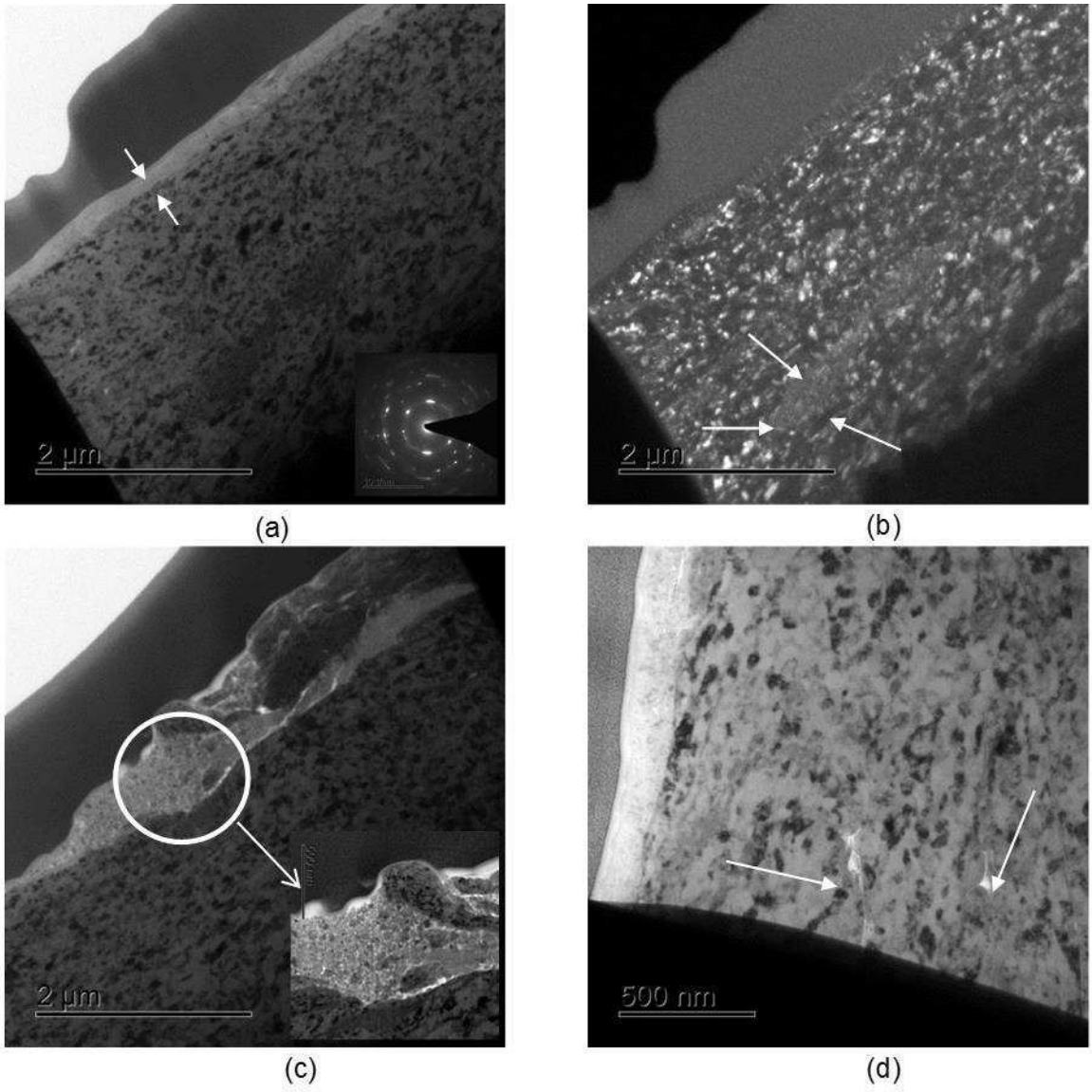

Figure 16

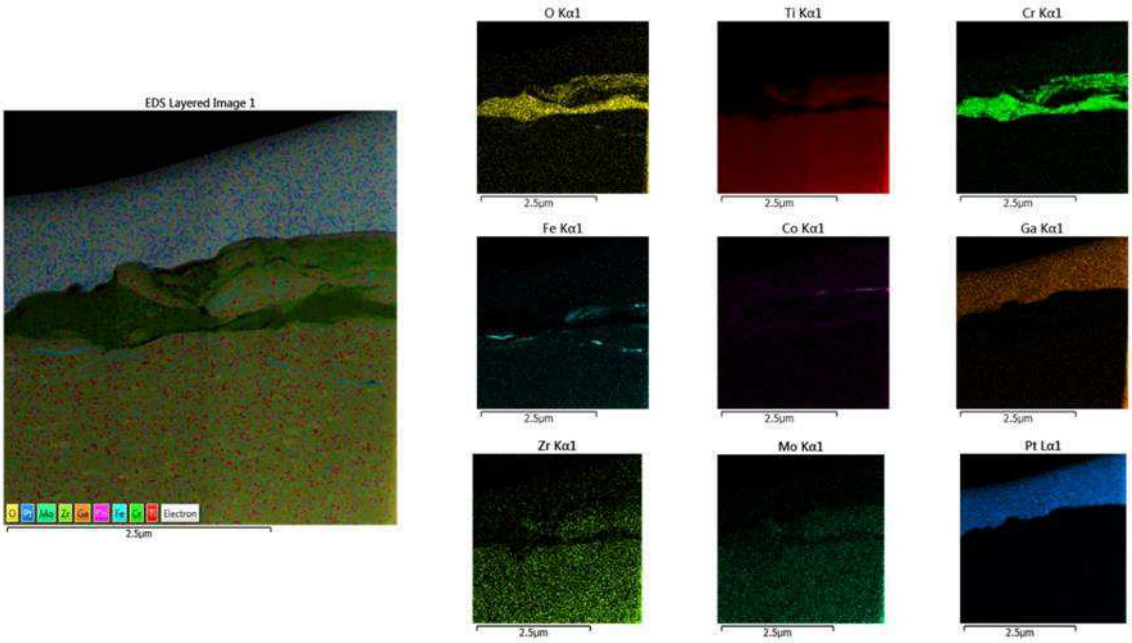

Figure 17

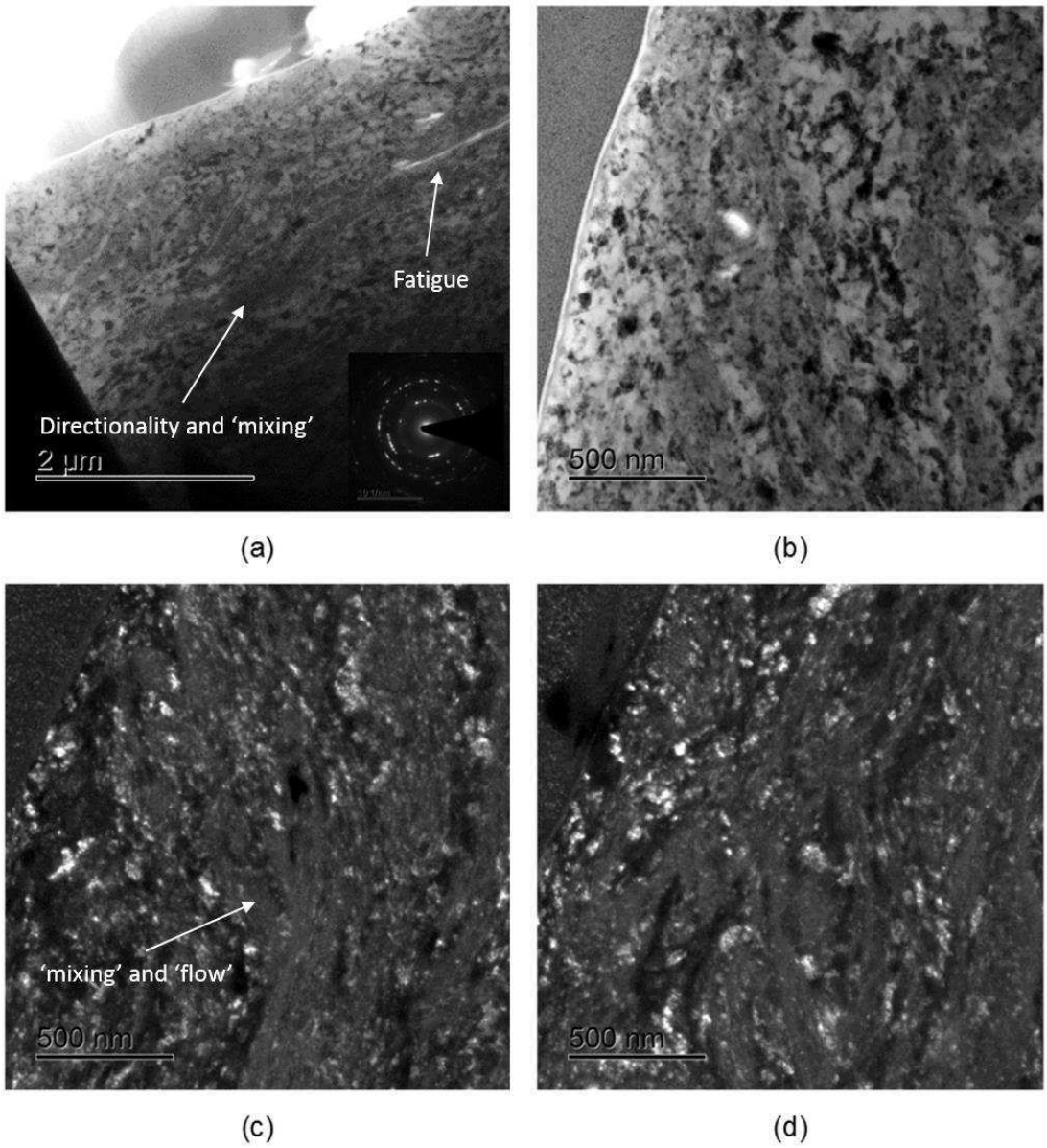

Figure 18

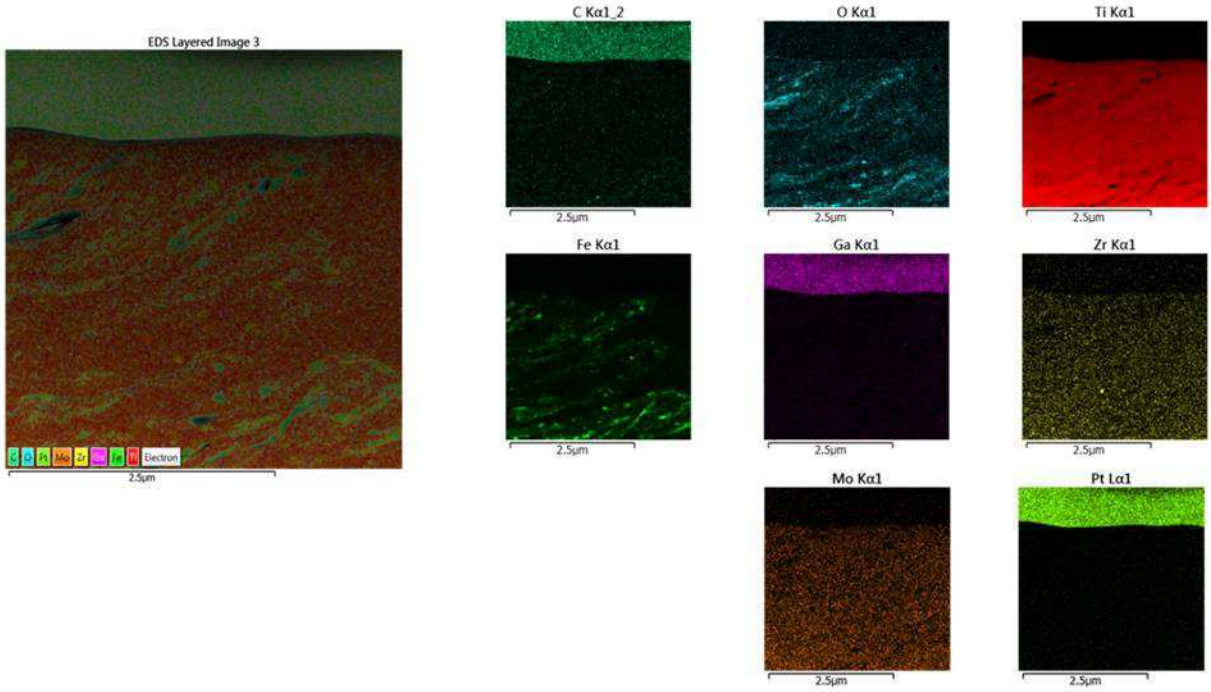

Figure 19

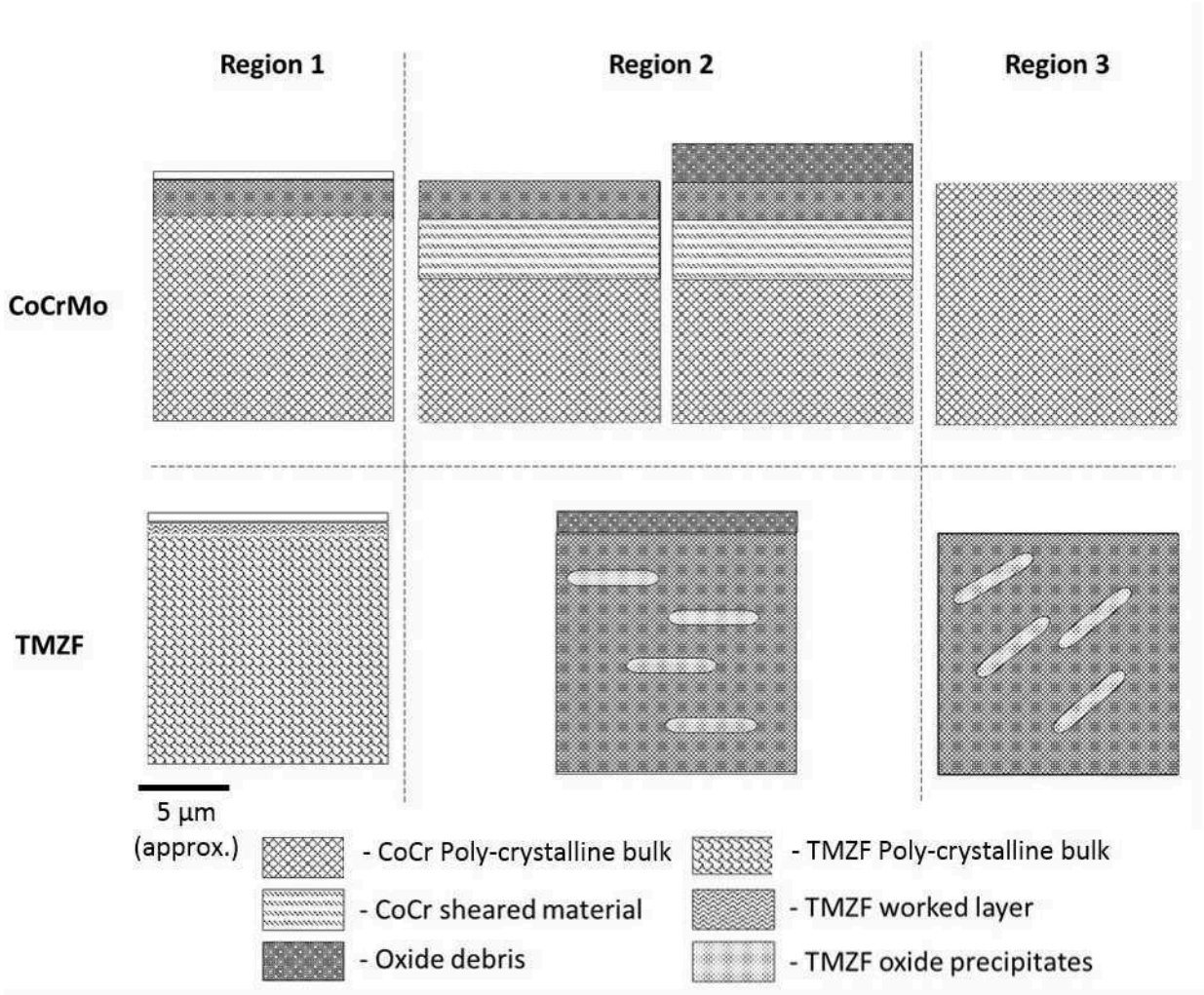

Figure 20

List of Tables

Table 1 – Chemical composition of the localised areas observed on the TMZF surface

Element	**Wt%**			
	Spectrum	**Spectrum**	**Spectrum**	**Spectrum**
	1	**2**	**3**	**4**
C	16.92	40.25	24.09	51.33
O	30.42	27.97	33.56	32.61
Si	2.31	2.57	0.77	4.96
P	0.72	0.45	-	0.60
Ti	20.66	-	16.42	-
Cr	7.10	-	7.02	-
Fe	2.02	-	-	5.43
Co	1.27	-	3.90	-
Cu	1.17	-	-	-
Zn	1.62	-	-	-
Zr	3.90	-	3.84	-
Mo	11.88	3.63	9.81	4.41
Ca	-	25.13	-	-
Cl	-	-	0.58	-
Al	-	-	-	0.65

Highlights

- Advanced surface analytical techniques have been applied to a retrieved bi-modular total joint replacement.
- A combination of surface analytical techniques have been used to study the changes in topography and sub surface microstructure due to tribocorrosion at the modular taper interface.
- Gross plastic deformation of the CoCrMo and TMZF alloy surfaces was seen. This varied depending on interface location.
- TEM-EDS demonstrated ‘mechanical alloy’ processes on the TMZF surface. This is hypothesised to change the interfacial properties resulting in degradation of the CoCrMo surface.